Structure of Serine Acetyltransferase in Complexes with CoA and Its Cysteine Feedback Inhibitor[†,‡]

Laurence R. Olsen, Bin Huang, Matthew W. Vetting, and Steven L. Roderick*

Department of Biochemistry, Albert Einstein College of Medicine, 1300 Morris Park Avenue, Bronx, New York 10461

Received October 14, 2003; Revised Manuscript Received March 12, 2004

ABSTRACT: Serine acetyltransferase (SAT, EC 2.3.1.30) catalyzes the CoA-dependent acetylation of the side chain hydroxyl group of L-serine to form *O*-acetylserine, as the first step of a two-step biosynthetic pathway in bacteria and plants leading to the formation of L-cysteine. This reaction represents a key metabolic point of regulation for the cysteine biosynthetic pathway due to its feedback inhibition by cysteine. We have determined the X-ray crystal structure of *Haemophilus influenzae* SAT in complexes with CoA and its cysteine feedback inhibitor. The enzyme is a 175 kDa hexamer displaying the characteristic left-handed parallel β-helix (LβH) structural domain of the hexapeptide acyltransferase superfamily of enzymes. Cysteine is bound in a crevice between adjacent LβH domains and underneath a loop excluded from the coiled LβH. The proximity of its thiol group to the thiol group of CoA derived from superimposed models of the cysteine and CoA complexes confirms that cysteine is bound at the active site. Analysis of the contacts of SAT with cysteine and CoA and the conformational differences that distinguish these complexes provides a structural basis for cysteine feedback inhibition, which invokes competition between cysteine and serine binding and a cysteine-induced conformational change of the C-terminal segment of the enzyme that excludes binding of the cofactor.

Serine acetyltransferase (SAT,[1] EC 2.3.1.30) catalyzes the CoA-dependent acetylation of the side chain hydroxyl group of L-serine to form *O*-acetylserine (*1*). This reaction is the first step in a two-step reaction pathway for L-cysteine biosynthesis from L-serine as found in bacteria, fungi, and higher plants. The second enzyme of this pathway, *O*-acetylserine sulfhydrylase (OASS), catalyzes the β-replacement of acetate with sulfide to convert *O*-acetylserine to L-cysteine (Scheme 1). SAT forms a bienzyme complex with OASS, termed cysteine synthase (CS) (*2*−*6*). Although the metabolic function of the bienzyme complex organization is not completely understood, its formation reduces V_{max} and increases the Michaelis constants for the substrates of OASS, alters its pH optimum, and may additionally stabilize SAT to thermal inactivation (*5*). Steady-state kinetic data for SAT are most consistent with sequential kinetic mechanisms (*5*, *7*−*9*).

Cysteine biosynthesis is the predominant means of incorporation of inorganic sulfur into bacterial biomolecules. The cysteine biosynthetic pathway of bacteria is regulated by several mechanisms, including feedback inhibition of SAT by cysteine (*1*, *4*, *5*, *10*) and transcriptional activation of a cysteine regulon composed of genes encoding the proteins of sulfur assimilation (*11*). Activation of the regulon is achieved through isomerization of *O*-acetylserine, the product of the SAT reaction, to *N*-acetylserine, which preferentially binds to the CysB activator to achieve induction, although the *cysE* gene encoding SAT itself appears to be expressed constitutively (*12*, *13*).

Scheme 1

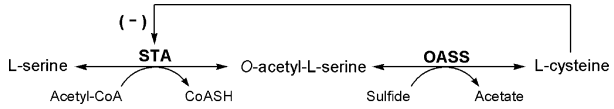

The 4000 metric ton worldwide demand for cysteine is currently met by a combination of chemical synthesis, hydrolysis of keratin, and fermentation. The quantity of cysteine that can be obtained by fermentation is limited by feedback inhibition of SAT and the rate at which cysteine is excreted into the medium. Bacteria and plants harboring feedback insensitive SAT have been identified by site-directed and PCR random mutagenesis (*14*−*19*), and characterization of these mutations points to an essential role for the C-terminal portion of the enzyme in conferring cysteine sensitivity (*17*, *20*). This region has also been implicated in CS complex formation, as C-terminal truncation mutants of SAT between 10 and 25 residues in length do not associate with OASS to form the bienzyme complex (*5*, *20*, *21*).

SAT is a member of the hexapeptide acyltransferase superfamily of enzymes that display imperfect tandem

[†] This work was supported by National Institutes of Health Grant AI42154 to S.L.R. M.W.V. was supported by Grant AI33696 to J. S. Blanchard.

[‡] Atomic coordinates have been deposited in the RCSB Protein Data Bank (entries 1SSM, 1SSQ, and 1SST).

* To whom correspondence should be addressed: Department of Biochemistry, Albert Einstein College of Medicine, 1300 Morris Park Ave., Bronx, NY 10461. Phone: (718) 430-2784. Fax: (718) 430-8565. E-mail: roderick@aecom.yu.edu.

[1] Abbreviations: ADA, *N*-(2-acetamido)-2-iminodiacetic acid; CoA, coenzyme A; CS, cysteine synthase bienzyme complex; DTT, dithioerythritol; LβH, left-handed parallel β-helix; MES, 2-(*N*-morpholino)-ethanesulfonic acid; MPD, 2-methyl-2,4-pentanediol; OASS, *O*-acetylserine sulfhydrylase; rms, root-mean-square; SAT, serine acetyltransferase.

10.1021/bi0358521 CCC: $27.50
Published on Web 04/30/2004

repeated copies of a six-residue periodicity theme that encode folding of an unusual left-handed parallel β-helix (LβH) structural domain (*22*−*25*). These enzymes act to transfer acetate, succinate, or long chain fatty acyl groups from their thioesters to a variety of structurally dissimilar acceptors bearing free amine or hydroxyl groups, including amino acids, antibiotics, cell wall components, and metabolic intermediates. The crystal structures of several hexapeptide acyltransferases have been determined in complexes with a variety of substrates (*25*−*34*).

Here, we describe the high-resolution crystal structure of the 175 kDa SAT from *Haemophilus influenzae* in complexes with CoA and inhibitory cysteine. These results define the overall polypeptide chain fold of the hexameric enzyme and the location of its active site. The interactions and conformational changes of SAT that accompany the binding of CoA and cysteine provide a structural basis for the phenomenon of cysteine feedback inhibition.

EXPERIMENTAL PROCEDURES

Overexpression, Purification, and Crystallization. The *cysE* gene encoding the serine acetyltransferase from *H. influenzae* (GenBank accession number P43886) was inserted into a pET3a expression vector and used to transform *Escherichia coli* BL21(DE3). Overexpressed SAT was purified by Poros 50 HQ ion exchange and Superdex 200 pg gel filtration chromatography. Electrospray mass spectrometry carried out on a purified sample was consistent with a nearly equimolar mixture of the full-length and *des*-Met polypeptides, presumably due to incomplete cleavage of the leader methionine residue by the host methionine aminopeptidase. To circumvent this problem, the T2N mutant was constructed by site-directed mutagenesis. Mass spectrometry demonstrated that the leader methionine of this mutant enzyme was completely uncleaved as expected from the known substrate specificity of the aminopeptidase (*35*). However, initial crystallization trials with this SAT as well as with the native enzyme were unsuccessful.

On the basis of the evident sequence similarity in the predicted LβH domain of SAT with other enzymes bearing hexapeptide repeat sequences, we surmised that residues beyond residue 242 of the 267-residue polypeptide were probably not included in the rigid LβH domain and might adopt a flexible conformation that could prevent crystallization. Indeed, the C-terminal portion of SAT from *E. coli* is required for association of the enzyme with OASS in formation of the bienzyme CS complex and is subject to proteolytic cleavage (*4*, *20*). A noncleavable N-terminal hexahistidine-tagged construct lacking the 25 C-terminal residues was overexpressed as the selenomethionyl protein and purified by Ni−NTA agarose chromatography. Crystals of this truncated variant were obtained by the hanging drop vapor diffusion method from 1:1 mixtures of a glycerol-stabilized protein containing 5 mM cysteine with a reservoir solution of 100 mM ADA (pH 6.0), 1−4% (v/v) MPD, and 190 mM Li_2SO_4. These crystals, termed form I, proved to lack bound cysteine. They belong to orthorhombic space group $P2_12_12$ and diffracted to 2.15 Å resolution at a synchrotron X-ray source.

A renewed effort to crystallize the T2N mutant of full-length SAT in the presence of cysteine yielded crystals from 1:1 mixtures of a protein containing 5 mM cysteine with a reservoir solution of 100 mM MES (pH 5.4), 20−40 mM $MgCl_2$, 2% (v/v) 2-propanol, and 5 mM DTT. These form II crystals belong to rhombohedral space group $R3$ and diffracted to 1.85 Å resolution using an in-house rotating anode X-ray generator.

To assess the location and conformation of substrates bound to the active site, a third crystal form was prepared. These crystals were prepared from 1:1 mixtures of the protein containing 50 mM CoA and 100 mM L-serine with a reservoir solution of 30% (v/v) polyethylene glycol 400 and 0.13 M LiCl. These form III crystals belong to orthorhombic space group $C222_1$ and diffracted to 2.0 Å resolution using the in-house X-ray facility.

X-ray Data Measurement and Structure Determinations. Selenomethionyl-truncated SAT crystals (form I) were subjected to multiple-wavelength anomalous diffraction (MAD) data measurement at beamline X9A of the National Synchrotron Light Source (Brookhaven National Laboratory, Upton, NY). The diffraction data were reduced with HKL (*36*). An initial set of selenium positions was identified with SnB version 2.1 (*37*) and was expanded by inspection of anomalous difference Fourier maps. Refinement of the selenium atomic parameters, phase calculation, and solvent flattening were carried out with SOLVE/RESOLVE (*38*, *39*). Although X-ray data corresponding to three wavelengths were measured, the highest-quality electron density map was produced by using only the peak wavelength in phasing procedures. A partially complete model was auto-built into an unaveraged map with MAID (*40*). Further model building and atomic parameter refinements were carried out with O (*41*) and CNS (*42*), employing thermal factor restraints. The final atomic model of the truncated apoenzyme SAT was refined to a crystallographic R_{factor} of 21.1% at 2.15 Å resolution (R_{free} = 25.8%) (Table 1).

X-ray diffraction data to 1.85 Å resolution were measured from a single crystal of full-length SAT (T2N mutant) at 125 K using an in-house Rigaku R-Axis IV^{++} image plate detector and RU-H3R rotating anode X-ray generator equipped with Osmic Blue optics and operating at 50 kV and 100 mA. The structure was determined by molecular replacement with EPMR (*43*) using one subunit from each trimer of the newly determined apoenzyme structure as the search model. The final atomic model of full-length SAT in complex with cysteine was refined to a crystallographic R_{factor} of 20.3% at 1.85 Å resolution (R_{free} = 26.1%). Similar methods were used to determine the structure of the form III crystals. This final atomic model of SAT bound to CoA was refined to a crystallographic R_{factor} of 22.3% at 2.0 Å resolution (R_{free} = 27.0%).

RESULTS

Atomic Model of SAT. The atomic model corresponding to the form I crystals of truncated SAT includes residues 1−240 of the 242-residue crystallized polypeptide for each of six crystallographically independent subunits of the hexameric molecule. Electron density corresponding to the uncleaved 11-residue N-terminal histidine tag and the last two residues of the truncated construct was not apparent for any subunit. Two residues consistently appear in the disallowed or generously allowed regions of the Ramachandran

Table 1: Data Measurement and Refinement Statistics[a]

	apoenzyme	cysteine	CoA
crystal form	I	II	III
space group	$P2_12_12$	$R3$	$C222_1$
unit cell parameters (Å)	$a = 107.1$ $b = 126.6$ $c = 107.3$	$a = b = 97.5$ $c = 108.5$	$a = 111.3$ $b = 125.0$ $c = 103.0$
no. of unique subunits	6	2	3
residue range crystallized	His tag−242 (truncated)	1−267 (T2N)	cleaved His tag; 1−267
residue range in the final model	1−240 (all subunits)	1−241 (short) 1−257 (long)	1−181; 189−240 1−181; 187−240 1−181; 186−240
	Data Measurement and Phasing		
X-ray wavelength (Å)	0.979	1.5418 (Cu Kα)	1.5418 (Cu Kα)
resolution (Å)	2.15	1.85	2.00
no. of observed reflections	914121	281849	143680
no. of unique reflections	147732	32779	44011
R_{merge} (%)	7.6 (26.7)	8.3 (21.8)	2.9 (15.3)
completeness (%)	94.7 (86.6)	99.9 (99.5)	90.2 (88.8)
figure of merit (2.23 Å)	0.25	−	−
no. of protein atoms	10962	3801	5393
no. of inhibitor/substrate atoms	−	14 (two cysteines)	144 (three CoAs)
no. of Mg^{2+} ions	−	2	−
no. of water molecules	468	378	172
average thermal factor (Å^2)			
protein atoms	27.7	20.1	34.3
inhibitor atoms	−	21.8	44.7
Mg^{2+} ions	−	20.8	−
water molecules	30.2	27.5	35.4
rms deviation from ideality			
Ramachandran allowed (%)	98.5	99.0	98.6
Ramachandran disallowed (%)	1.5	1.0	1.4
bond lengths (Å)	0.012	0.012	0.013
bond angles (deg)	1.8	1.6	1.7
R_{factor}/R_{free} (%)	21.1/25.8 (24.1/31.8)	20.3/26.1 (25.1/31.3)	22.3/27.0 (25.9/29.7)

[a] Data measurement statistics for the selenomethionyl apoenzyme crystal refer to unmerged anomalous measurements. $R_{merge} = \sum|I_i - \langle I\rangle|/\sum|I_i| \times 100$. The figure of merit for the 2.23 Å resolution single-wavelength anomalous diffraction (SAD) phase determination was calculated prior to density modification procedures. Ramachandran allowed refers to the percentage of residues residing in the most favored and additionally allowed regions of the Ramachandran plot, as defined by PROCHECK (*45*). Ramachandran disallowed refers to the percentage of residues in the generously allowed and disallowed regions. $R_{factor} = \sum|F_o - F_c|/\sum|F_o| \times 100$ for all available data, but excluding data reserved for the calculation of R_{free}. $R_{free} = \sum|F_o - F_c|/\sum|F_o| \times 100$ for a 5% subset of X-ray diffraction data omitted from refinement calculations. Values in parentheses refer to the corresponding statistic calculated for data in the highest-resolution bin.

plot (*44*, *45*) in the SAT structures determined here, His-154 and Ala-155, although the conformations of both residues are supported by excellent quality electron density.

The asymmetric unit of the form II crystals contains two subunits of the 267-residue full-length enzyme. These two subunits (one from each trimer) form the complete hexameric molecule after repetition by a crystallographic 3-fold axis. The refined atomic model includes residues 1−241 and 1−257 from the two subunits.[2] These subunits are termed the short and long subunits, respectively. Because neither subunit displayed electron density corresponding to the full-length polypeptide, several form II crystals were dissolved for analysis by electrospray mass spectrometry, which confirmed that these crystals were indeed composed of the full-length protein (observed value of 29 176 Da, calcd value of 29 180 Da). The atomic model for the form II full-length crystals also includes two molecules of cysteine and two Mg^{2+} ions.

The asymmetric unit of the form III crystals contains one-half of the native hexameric molecule (as one trimer) and three molecules of CoA. These three subunits lack interpretable electron density corresponding to residue ranges of 182−188, 182−186, and 182−185 as well as for any residue beyond residue 240 of the 267-residue protein. Although 100 mM L-serine was included in the crystallization experiment, no electron density was found that could be attributed to this substrate.

Overall Polypeptide Chain Fold of SAT. The overall structure of residues 1−257 of the long subunit, derived from form II crystals containing the full-length enzyme, can be subdivided into an N-terminal domain (residues 1−136), a coiled LβH domain (residues 137−232), and a C-terminal segment (residues 241−257) (Figure 1). The N-terminal domain is composed of eight α-helices: α1 (residues 2−19), α2 (23−33), α3 (37−49), α4 (55−70), α5 (72−87), α6 (95−100), α7 (101−118), and α8 (121−136). The repetition of helices α2−α4 by the molecular 3-fold axis forms a surface which packs against the cognate surface of the

[2] Subunits A−C form one trimer and subunits D−F the opposite trimer of the hexameric molecule. The asymmetric unit of the form II crystals is composed of one subunit from each trimer, called the long subunit and short subunit. Although these crystals are of the T2N mutant of the 267-residue full-length protein, only residues 1−241 (short subunit) and residues 1−257 (long subunit) have been modeled. Each active site is formed at the junction of two adjacent subunits of a trimer. When a single active site is described, these two subunits are termed A and B. The A subunit forms the left side of the active site, and the B subunit is on the right when viewed from afar and with the N-terminal end of the β-helix directed upward (e.g., the purple and blue subunits, respectively, of Figures 1A and 5).

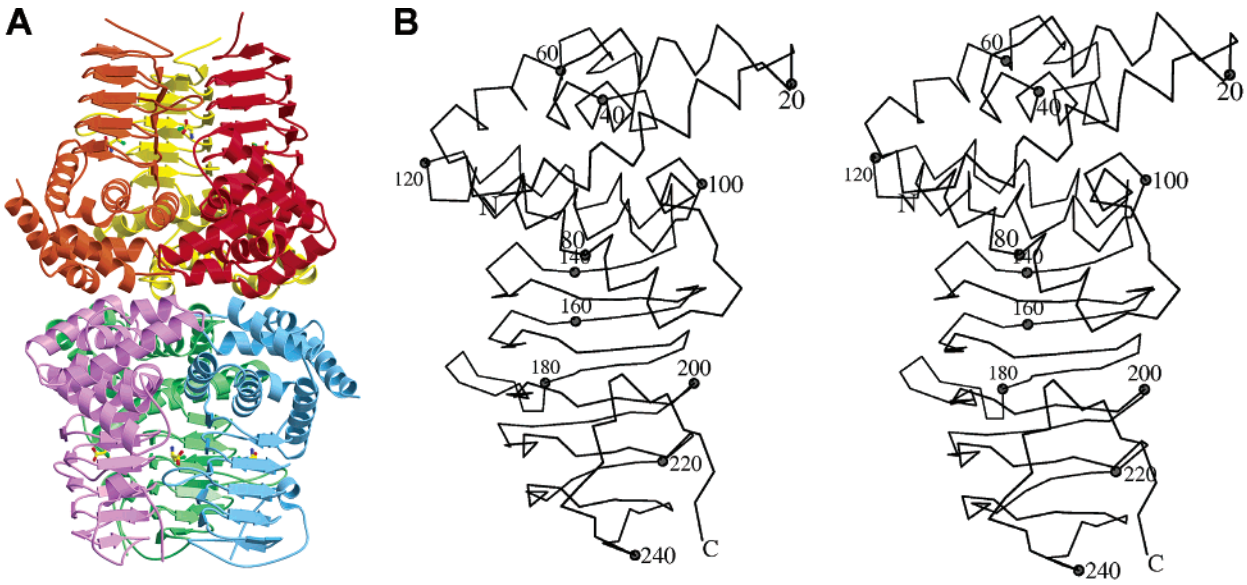

FIGURE 1: (A) Ribbon diagram of hexameric serine acetyltransferase bound to cysteine. The bottom trimer (blue, green, and purple) corresponds to the long subunit and displays the conformation of the C-terminal segment (residues 241−257). This segment could not be modeled in the top trimer (red, yellow, and orange) which is termed the short subunit. (B) Stereoview α-carbon trace of a single subunit. The direction of view is the same as that for the purple subunit in panel A. This figure was prepared with MOLSCRIPT (*49*), BOBSCRIPT (*50*), Raster3D (*51*), and PyMOL (*52*).

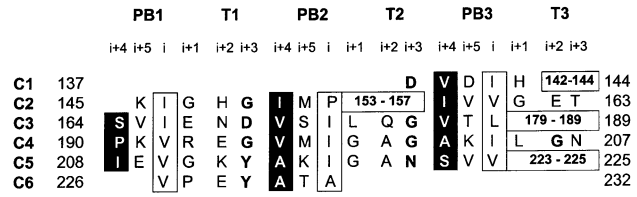

FIGURE 2: Structure-based amino acid sequence alignment of the LβH domain of SAT (residues 137−232) identifying structurally equivalent residues in each of the six coils. Each horizontal line represents one complete or partial coil. The parallel β-strands that form the planar faces of the LβH are denoted PB1−PB3, and the turns separating these strands are denoted T1−T3. The conserved hydrophobic residues at position *i* are boxed. Residues in the left-handed conformation at position $i + 3$ (main chain torsion angle $\varphi > 0$) are depicted in bold type. The small residues at the corners of each coil at position $i + 4$ are inversely shaded. Residues 179−189 are not included in the coiled β-helix and form the extended LβH loop.

opposing trimer to form the loose dimer-of-trimers structure of the hexameric enzyme. The LβH domain of SAT is formed predominantly by partial or complete copies of six left-handed β-helical coils (Figure 2). Although each complete coil is based on three tandem-repeated hexapeptide units, the observed length of a single coil often differs from the length of the canonical 18-residue coil due to the insertion of LβH loops that disobey the hexapeptide repeat sequence rule. One of two such LβH loops (residues 179−189) projects from coil 3 into the space between two adjacent LβH domains. This extended LβH loop is partly disordered in the apoenzyme structure obtained from the form I crystals and is largely absent in all three independent subunits of the CoA complex structure. The C-terminal segment of SAT is seen at its greatest length from residue 241 to 257 in the long subunit of the form II (cysteine-bound) crystals. Crystal contacts with α1 and α5 of an adjacent hexamer may prevent this segment from adopting a similar conformation in the short subunit. Residues beyond residue 240 are absent from the model for all subunits of the CoA complex structure. The C-terminal segment contains a short α-helix (residues 247−252) that contacts the LβH domain of the same subunit. There is no significant electron density corresponding to the 10 C-terminal residues of SAT (258−267) in any of the structures described here.

The quaternary structure of all known hexapeptide acyltransferases is trimeric with the exception of SAT, which had been predicted to adopt a hexameric structure, based on equilibrium sedimentation studies and the appearance of electron micrographs of negatively stained particles (*46*). It was therefore expected that the quaternary structure of SAT would be hexameric, based on dimerization of the widely conserved trimeric structure of the hexapeptide acyltransferase superfamily of enzymes. The three crystal forms studied here placed an entire hexamer, one-third of a hexamer, and one-half of a hexamer in the asymmetric unit of the unliganded, cysteine-bound, and CoA-bound crystals, respectively. Superposition of the Cα positions of the two complex structures indicates that the overall conformation of the N-terminal α-helical domain differs more significantly than the superimposed structures of the LβH domain (rms deviations of 1.6 and 0.6 Å, respectively). The source of these differences is not obvious from inspection of the superimposed models, but might result from differences in the binding of Asp-88A to the cysteine inhibitor amino group (see below), crystal packing interactions, or differences in crystallization conditions.

Structure of SAT Bound to Cysteine. The 1.85 Å resolution electron density maps for the full-length form II crystals clearly indicated the presence of a single cysteine molecule bound to both the long and short subunits (Figure 3A). The location of the bound cysteine molecule, its conformation, and most of its interactions with the enzyme are identical for the two crystallographically independent subunits. The cysteine binding pocket is located between the adjacent LβH domains of subunits termed A and B.[2] It accepts interactions from the extended LβH loop (residues 179B−189B), a loop joining helices α5 and α6 (residues 88A−94A), and an

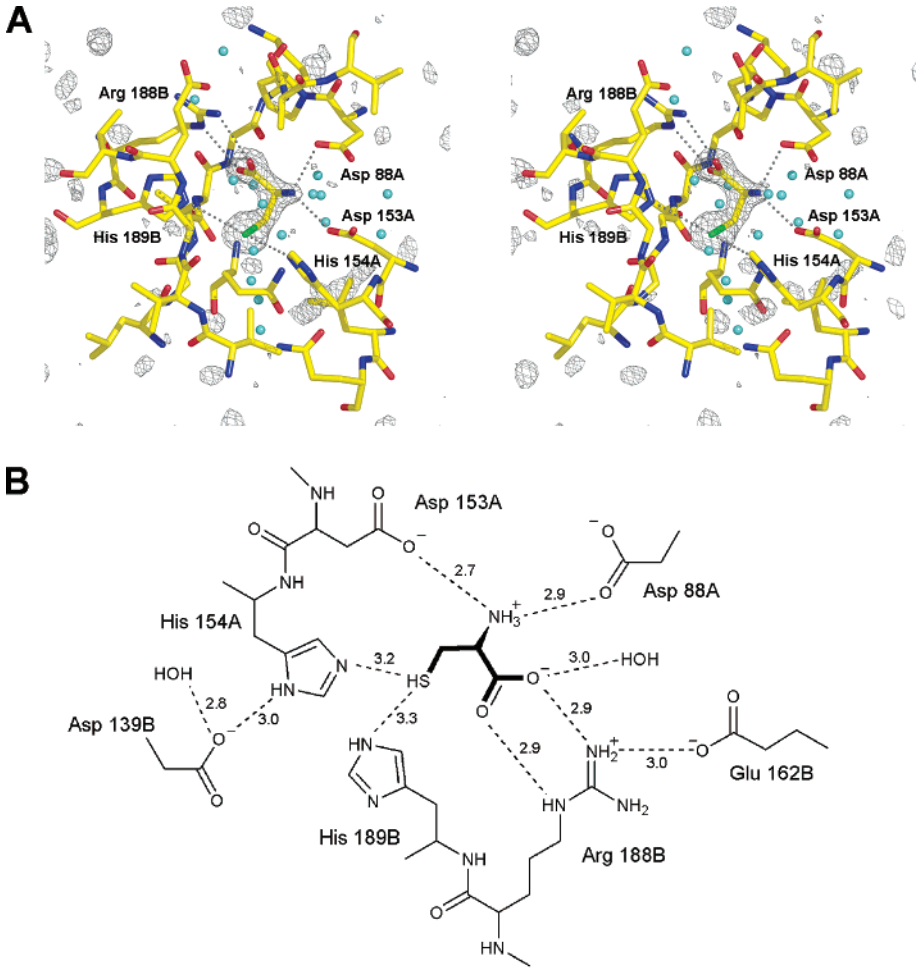

FIGURE 3: (A) Stereoview of the active site of SAT with bound cysteine. The direction of view is equivalent to that of Figure 1A. The electron density is from an $F_o - F_c$ map contoured at 3.5σ prior to the initial fitting and refinement of the atomic coordinates corresponding to cysteine. The coordinates are from the final refined model corresponding to the form II crystals. (B) Schematic depiction of the interactions of SAT with bound cysteine shared by the long and short subunits. Protonation states are arbitrary. Hydrophilic interactions are represented by dashed lines with interatomic distances in angstroms.

additional LβH loop inserted at the T2 turn position of LβH coil 2 (residues 153A−157A) (Figure 3). The amino group of the inhibitor is bound by the side chains of Asp-88A and Asp-153A. The carboxyl group makes two interactions with the side chain of Arg-188B. The carboxyl forms an additional interaction with a water molecule. The sulfhydryl is wedged between His-154A and His-189B and interacts with the imidazole ring NE2 group of each. An interaction of the sulfhydryl group with the peptide nitrogen of Gly-180B is formed only in the long subunit, for which the conformation of the LβH loop bearing this residue differs from the conformation of the short subunit due to its interactions with the C-terminal segment.

Structure of SAT Bound to CoA. The 2.0 Å resolution structure of the form III crystals of SAT prepared in the presence of CoA and L-serine identifies the structure of the enzyme extending to only residue 240, lacking the 27 C-terminal residues for each of the three crystallographically independent subunits. The CoA is bound in a crevice between β-helices at three equivalent active site locations related by a 3-fold axis. These three active sites are related to the three remaining active sites of the hexameric molecule by a crystallographic 2-fold rotation. No electron density corresponding to serine was found, despite its inclusion in the crystallization experiment. The carbonyl groups of the cofactor pantetheinyl arm accept hydrogen bonds from Ala-200A and Ala-218A, two residues occupying structurally equivalent positions in adjacent coils of the LβH domain (Figures 2 and 4). The amide nitrogen groups of the cofactor donate hydrogen bonds to the peptide oxygens of Gly-180B and Thr-181B. These hydrogen bonds stabilize an extended conformation of the pantetheine arm and direct its thiol toward the side chains of His-154A (distance of 3.6 Å) and Gln-174A (3.6 Å).

DISCUSSION

The SAT from *H. influenzae* was studied as the truncated enzyme (form I crystal) and as the full-length polypeptide in complexes with cysteine (form II) and CoA (form III). Because the C-terminal truncation of SAT is located at the active site, we focus attention on the structures of the full-length enzyme bound in complexes to cysteine and CoA. A least-squares superposition of the cysteine and CoA complex structures was carried out with an rms discrepancy of 0.6 Å for 85 Cα atoms of the coiled LβH domain. This superposition places the thiol groups of cysteine and CoA within 2.9 Å of one another. Both of these thiol groups are situated close to the NE2 group of His-154A (3.2 and 3.6 Å, respectively), one of two residues (with Ala-155) that consistently appear in the generously allowed or disallowed

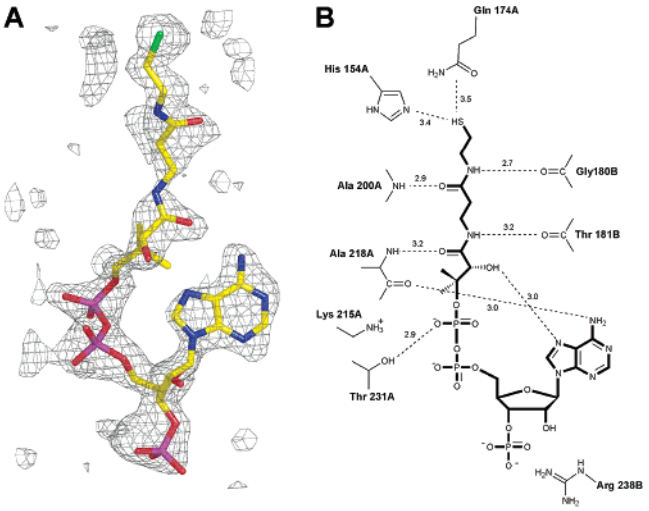

FIGURE 4: (A) Experimental electron density due to CoA. The electron density is from an $F_o - F_c$ map contoured at 2.0σ prior to the initial fitting and refinement of the atomic coordinates corresponding to CoA. The coordinates are from the final refined model corresponding to the form III crystals. (B) Schematic depiction of the interactions of SAT with bound CoA. Hydrophilic interactions are represented by dashed lines with interatomic distances in angstroms.

regions of the Ramachandran plot, indicative of energetically unfavorable main chain torsion angle pairs. The location of the cysteine binding pocket between two adjacent LβH domains and in the proximity of the CoA thiol is identical to that of the substrate acceptor binding pockets of four additional hexapeptide acetyltransferases, which share these binding characteristics and similarly make use of residues contributed from coils 1 and 2 of the LβH to bind their acceptors (*27*−*29*, *47*). These results confirm that the cysteine feedback inhibitor binds to the active site of SAT.

The superposition of the cysteine and CoA complexes also demonstrates that the C-terminal segment (residues 241A−257A) of the cysteine complex and the pantetheinyl arm of CoA compete for binding to the extended LβH loop (residues 179B−189B) (Figure 5). In particular, residues 254A−257A occupy the same position as the pantetheinyl arm of CoA with the hydrophobic side chain of Phe-256A accommodated in the same pocket as is the adenine moiety of the cofactor. In addition, Gly-180B and Thr-181B of the extended LβH loop engage in a different set of interactions in the two complexes. In the cysteine complex, the Gly-180B nitrogen interacts with the cysteine thiol while the side chain of Thr-181B accepts a hydrogen bond from the peptide group of Gln-254A of the C-terminal segment. In the CoA complex, however, the C-terminal segment of the enzyme is displaced by CoA. The peptide oxygens of Gly-180B and Thr-181B instead accept hydrogen bonds from the two pantetheinyl amide groups of the cofactor. The K_i of 1 μM for cysteine is in part explained by this interaction of the C-terminal segment with the extended LβH loop. Binding of the inhibitor to SAT reduces its solvent accessible surface area by 93% and leaves no apparent diffusion path from the enzyme in the absence of a conformational change. Such a conformational change of the extended LβH loop would be inhibited by its interaction with the C-terminal segment.

The importance of this interaction between the extended LβH loop and the C-terminal segment is underscored by the spatial clustering of residue positions that have been observed to confer the cysteine/cystine overproduction phenotype (*5*, *14*−*21*, *48*). These mutant strains are of commercial interest for the high-level production of cysteine by fermentation. PCR random mutagenesis of the *E. coli cysE* gene encoding SAT identified six such single or double mutants, including (*H. influenzae* numbering) E162G/M197V, T163K, M197R, M197T, P248R, and A(S in *E. coli*)249L involving five different residues (henceforth italicized) (*15*). *Glu-162B* interacts with the side chain of Arg-188B which binds the cysteine carboxyl group. The side chain hydroxyl of *Thr-163B* accepts hydrogen bonds from the peptide nitrogens of Arg-188B and His-189B as well as the ND1 group of His-189B, two residues that directly contact cysteine. Independently screened *E. coli cysE* mutants also identified this threonine residue in a T163A/G(S in *H. influenzae*)241S double mutant with several 100-fold decreased cysteine sensitivity (*48*). *Met-197A* contacts Pro-248A of the C-terminal segment. *Pro-248A* and *Ala-249A* are residues of the C-terminal segment that interacts directly with the LβH loop. The homologue of *Ala-249A* in the SAT from watermelon, Gly-277, is a residue that was deemed to be primarily responsible for the feedback inhibition of a cysteine sensitive isoform (*14*). Furthermore, genetic truncation of the 20 C-terminal residues of *E. coli* SAT or the mutation of *E. coli* Met-256 to any of 17 residue types also reduces cysteine feedback sensitivity (*16*, *17*). The residue equivalent to *E.*

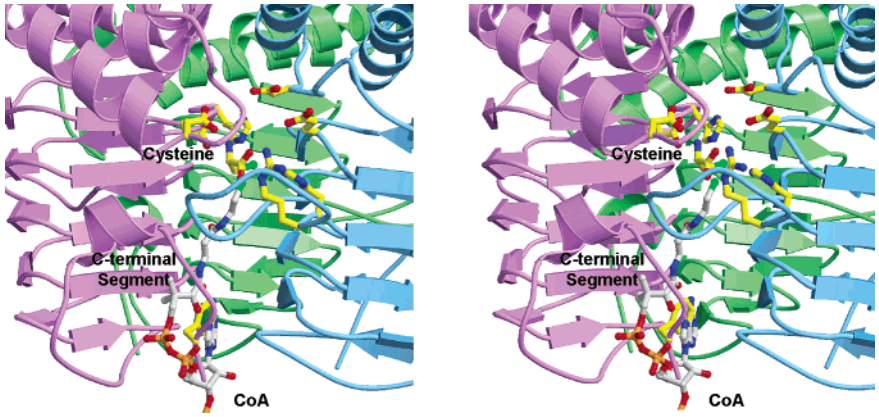

FIGURE 5: Stereoview superposition of CoA (gray bonds) from the CoA-bound structure of SAT onto the cysteine-bound structure of the enzyme. The C-terminal segment is displaced in the structure of SAT bound to CoA, due to the steric overlap of the CoA pantetheinyl arm with the C-terminal segment. The overlap of the adenine group of CoA and the hydrophobic side chain of Phe-256 is depicted.

coli Met-256 is *H. influenzae* Met-252, which resides in a short α-helix within the C-terminal segment. Hence, the homologues of the residues responsible for the cysteine/cystine overproduction phenotype (*Glu-162*, *Thr-163*, *Met-197*, *Pro-248*, and *Ala-249*) all contact the LβH loop or the C-terminal segment directly or are members of the C-terminal segment.

Kinetic and calorimetric studies confirm that cysteine binding reduces the affinity of serine and acetyl-CoA for the SATs from *E. coli* (70% of its sequence identical with that of *H. influenzae* SAT) (*1*, *4*, *10*) and *H. influenzae* (C. M. Johnson and P. F. Cook, personal communication). That the cysteine and serine binding sites overlap is supported by kinetic and microcalorimetric data obtained with serine analogues (*10*). Taken together, the kinetic and binding data are consistent with the structural results obtained here and point to a complex mechanism of cysteine feedback inhibition. This mechanism invokes direct competition between cysteine and serine binding as well as a reduction in the affinity of the enzyme for acetyl-CoA promoted by a conformational change of the C-terminal segment as it interacts with the cysteine-bound extended LβH loop. The mutually exclusive binding of cysteine with both substrates of the enzyme would lead to the inhibition of both serine acetylation and acetylation of the inhibitor.

ACKNOWLEDGMENT

We acknowledge Paul F. Cook (University of Oklahoma, Norman, OK) for helpful discussions.

REFERENCES

1. Kredich, N. M., and Tomkins, G. M. (1966) *J. Biol. Chem. 241*, 4955−4965.
2. Kredich, N. M., and Tomkins, G. M. (1967) in *Organizational Biosynthesis* (Vogel, H. J., Lampen, J. O., and Bryson, V., Eds.) pp 189−198, Academic Press, New York.
3. Becker, M. A., Kredich, N. M., and Tomkins, G. M. (1969) *J. Biol. Chem. 244*, 2418−2427.
4. Kredich, N. M., Becker, M. A., and Tomkins, G. M. (1969) *J. Biol. Chem. 244*, 2428−2439.
5. Mino, K., Yamanoue, T., Sakiyama, T., Eisaki, N., Matsuyama, A., and Nakanishi, K. (2000) *Biosci., Biotechnol., Biochem. 64*, 1628−1640.
6. Wirtz, M., Berkowitz, O., Droux, M., and Hell, R. (2001) *Eur. J. Biochem. 268*, 686−693.
7. Leu, L.-S., and Cook, P. F. (1994) *Biochemistry 33*, 2667−2671.
8. Leu, L.-S., and Cook, P. F. (1994) *Protein Pept. Lett. 1*, 157−162.
9. Hindson, V. J., and Shaw, W. V. (2003) *Biochemistry 42*, 3113−3119.
10. Hindson, V. J. (2003) *Biochem. J. 375*, 745−752.
11. Kredich, N. M. (1996) in *Escherichia coli and Salmonella Cellular and Molecular Biology* (Curtiss, R., Ingraham, J. L., Lin, E. C. C., Low, K. B., Magasanik, B., Reznikoff, W. S., Riley, M., Schaechter, M., and Umbarger, H. E., Eds.) pp 514−527, American Society for Microbiology, Washington, DC.
12. Kredich, N. M. (1971) *J. Biol. Chem. 246*, 3474−3484.
13. Jones-Mortimer, M. C., Wheldrake, J. F., and Pasternak, C. A. (1968) *Biochem. J. 107*, 51−53.
14. Inoue, K., Noji, M., and Saito, K. (1999) *Eur. J. Biochem. 266*, 220−227.
15. Takagi, H., Kobayashi, C., Kobayashi, S., and Nakamori, S. (1999) *FEBS Lett. 452*, 323−327.
16. Nakamori, S., Kobayashi, S. I., Kobayashi, C., and Takagi, H. (1998) *Appl. Environ. Microbiol. 64*, 1607−1611.
17. Denk, D., and Bock, A. (1987) *J. Gen. Microbiol. 133* (Part 3), 515−525.
18. Takagi, H., Awano, N., Kobayashi, S., Noji, M., Saito, K., and Nakamori, S. (1999) *FEMS Microbiol. Lett. 179*, 453−459.
19. Wirtz, M., and Hell, R. (2003) *Amino Acids 24*, 195−203.
20. Mino, K., Yamanoue, T., Sakiyama, T., Eisaki, N., Matsuyama, A., and Nakanishi, K. (1999) *Biosci., Biotechnol., Biochem. 63*, 168−179.
21. Mino, K., Hiraoka, K., Imamura, K., Sakiyama, T., Eisaki, N., Matsuyama, A., and Nakanishi, K. (2000) *Biosci., Biotechnol., Biochem. 64*, 1874−1880.
22. Downie, J. A. (1989) *Mol. Microbiol. 3*, 1649−1651.
23. Vaara, M. (1992) *FEMS Microbiol. Lett. 97*, 249−254.
24. Dicker, I. B., and Seetharam, S. (1992) *Mol. Microbiol. 6*, 817−823.
25. Raetz, C. R. H., and Roderick, S. L. (1995) *Science 270*, 997−1000.
26. Beaman, T. W., Binder, D. A., Blanchard, J. S., and Roderick, S. L. (1997) *Biochemistry 36*, 489−494.
27. Beaman, T. W., Sugantino, M., and Roderick, S. L. (1998) *Biochemistry 37*, 6689−6696.
28. Sugantino, M., and Roderick, S. L. (2002) *Biochemistry 41*, 2209−2216.
29. Wang, X.-G., Olsen, L. R., and Roderick, S. L. (2002) *Structure 10*, 581−588.
30. Brown, K., Pompeo, F., Dixon, S., Mengin-Lecreulx, D., Cambillau, C., and Bourne, Y. (1999) *EMBO J. 18*, 4096−4107.
31. Kostrewa, D., D'Arcy, A., Takacs, B., and Kamber, M. (2001) *J. Mol. Biol. 305*, 279−289.
32. Olsen, L. R., and Roderick, S. L. (2001) *Biochemistry 40*, 1913−1921.
33. Sulzenbacher, G., Gal, L., Peneff, C., Fassy, F., and Bourne, Y. (2001) *J. Biol. Chem. 276*, 11844−11851.
34. Lo, L. L., Dal Degan, F., Poulsen, P., Andersen, S. M., and Larsen, S. (2003) *Biochemistry 42*, 5225−5235.
35. Ben-Bassat, A., Bauer, K., Chang, S.-Y., Myambo, K., Bossman, A., and Chang, S. (1987) *J. Bacteriol. 169*, 751−757.
36. Otwinoski, Z., and Minor, W. (1997) in *Methods in Enzymology* (Carter, C. W., Jr., and Sweet, R. M., Eds.) pp 307−326, Academic Press, New York.
37. Smith, G. D., Nagar, B., Rini, J. M., Hauptman, H. A., and Blessing, R. H. (1998) *Acta Crystallogr. D54* (Part 5), 799−804.
38. Terwilliger, T. C., and Berendzen, J. (1999) *Acta Crystallogr. D55* (Part 4), 849−861.
39. Terwilliger, T. C. (1999) *Acta Crystallogr. D55*, 1863−1871.
40. Levitt, D. G. (2001) *Acta Crystallogr. D57*, 1013−1019.
41. Jones, T. A., Zou, J.-Y., Cowan, S. W., and Kjeldgaard, M. (1991) *Acta Crystallogr. A47*, 110−119.
42. Brunger, A. T., Adams, P. D., Clore, G. M., DeLano, W. L., Gros, P., Grosse-Kunstleve, R. W., Jiang, J. S., Kuszewski, J., Nilges, M., Pannu, N. S., Read, R. J., Rice, L. M., Simonson, T., and Warren, G. L. (1998) *Acta Crystallogr. D54*, 905−921.
43. Kissinger, C. R., Gehlhaar, D. K., Smith, B. A., and Bouzida, D. (2001) *Acta Crystallogr. D57*, 1474−1479.
44. Ramachandran, G. N., Ramakrishnan, C., and Sasisekharan, V. (1963) *J. Mol. Biol. 7*, 95−99.
45. Laskowski, R. A., MacArthur, M. W., Moss, S. D., and Thornton, J. M. (1993) *J. Appl. Crystallogr. 26*, 283−291.
46. Hindson, V. J., Moody, P. C., Rowe, A. J., and Shaw, W. V. (2000) *J. Biol. Chem. 275*, 461−466.
47. Beaman, T. W., Blanchard, J. S., and Roderick, S. L. (1998) *Biochemistry 37*, 10363−10369.
48. Maier, T. H. (2003) *Nat. Biotechnol. 21*, 422−427.
49. Kraulis, P. J. (1991) *J. Appl. Crystallogr. 24*, 946−950.
50. Esnouf, R. M. (1997) *J. Mol. Graphics Modell. 15*, 132−134.
51. Merrit, E. A., and Murphy, M. E. P. (1994) *Acta Crystallogr. D50*, 869−873.
52. DeLano, W. L. (2002) *PyMOL*, DeLano Scientific, San Carlos, CA.

BI0358521